On Modeling JANUS Packet Errors over a Shallow Water Acoustic Channel using Markov and Hidden Markov Models

Beatrice Tomasi*, Paolo Casari*, Lorenzo Finesso§, Giovanni Zappa‡, Kim McCoy‡, Michele Zorzi*
*Department of Information Engineering, University of Padova, Italy — {tomasibe, casarip, zorzi}@dei.unipd.it
§ISIB–CNR, Padova, Italy — lorenzo.finesso@isib.cnr.it
‡NATO Undersea Research Centre (NURC), La Spezia, Italy — {zappa, mccoy}@nurc.nato.int

***Abstract*—In this paper, we investigate how to represent the packet error process in a shallow water acoustic channel by means of Markov as well as hidden Markov models. To train the models, we employ experimental traces taken from transmissions performed during the SubNet'09 sea trials, off the coast of Pianosa island, Italy. In particular, signal-to-noise ratio (SNR) time series show significant transitions of the average SNR on a large time scale, which motivates the use of hidden Markov models. The discussion on which model best fits this experimental data is carried out considering relevant metrics for networking, i.e., packet error rate (PER), length of error bursts and correlation of errors after a given number of packet transmissions. Results show that hidden Markov models yield accurate reproduction of both first and second-order metrics.**

I. Introduction

Due to very large operational and equipment costs involved in the setup of large-scale testbeds, simulation is still the most flexible tool for extensive characterization of underwater acoustic networks [1]. However, simulators frequently rely on simplified models of the underwater channel, e.g., considering single-path propagation [2], [3]. These models may help provide an order-of-magnitude prediction of the channel behavior and of the networking protocols operating on top of it, but usually assume the speed of sound as constant throughout the water column, and in addition do not include such important propagation effects as multipath-induced fading and time-varying channel behaviors. A different approach investigated in [4] aims at partially overcoming this fact by including a ray-model-based acoustic propagation simulator in the popular network simulator ns2. While this certainly improves the accuracy of the simulation, the required computational burden is potentially very high.

A possible way around this problem is to deduce synthetic channel models from, e.g., measured packet error traces taken from experimental campaigns. The drawback of such models is their dependence on boundary conditions expressed by environmental factors (e.g., water depth, sound speed profile, bathymetry, bottom sediments, surface waves), as well as by the type of modulation and receiver-side signal processing. However, if such conditions are at least similar to those affecting the traces used to train the models, networking protocols run on top of the channel model are expected to smooth out sufficiently small differences [5].

In this paper, we consider JANUS [6] packet transmissions performed throughout the summer of 2009. JANUS is a communications format designed for unsolicited broadcasting of relevant information regarding the sender of the signal (including, but not limited to, navigation information) by means of underwater acoustic communications. A deeper description of the JANUS waveform format is reported in Sec. II-A: for the moment suffice it to say that the signal includes a Cyclic Redundancy Check (CRC) code that can be employed to check the correctness of the packet, and a synchronization preamble which can be used for SNR estimation. We start from the relationship between SNR and packet error rate (PER) and show that a linear fit between the SNR (in dB) and the PER matches data satisfactorily. We also discuss the non-linear relationship between the transmitter-receiver distance and the obtained PER.

By observing the time series of SNR samples, we discuss the presence of quick changes in the average value, and investigate how to model the channel so that these changes can be captured, at least to some extent. To this end, we consider three different types of Markov models (namely, a 2-state model, a 4-state model extending the 2-state one by incorporating memory of one more past event, and a hidden 2-state Markov model), and compare such models against a plain independent and identically distributed (iid) error model. The latter is a standard model often assumed to hold in, e.g., network simulations, whenever deterministic propagation models are considered, and is used here as a term of comparison for the accuracy of Markov models. While the dataset currently available to us is limited and not sufficient to derive very general conclusions, the final aim is to show that such models can reproduce accurately enough the statistics of underwater channels subject to the same environmental conditions. This would make them amenable to be eventually embedded into more complex network simulators, where they would provide a compact and computationally efficient method of reproducing the statistics of links showing similar environmental characteristics (depth, distance, sound speed profile, etc.) to those studied in this paper.

II. Testbed Setup and Data Set description

A. Scenario and transmitted signal format

The sea trials took place in the framework of SubNet 2009, whose main goal was to experiment the transmission of JANUS waveforms [6]. These are digitally modulated frequency hopping-binary frequency shift keying (FH-BFSK) signals, transmitted in the 9-$14\,\mathrm{kHz}$ band. The signals are composed of a preamble (three wakeup tones plus a $400\,\mathrm{ms}$ silence plus a hyperbolic band-sweeping chirp), a further $200\,\mathrm{ms}$ silence and the actual packet, which in turn is formed by a header containing actual JANUS data and an optional payload. A later JANUS version eliminates one of the silences by substituting the hyperbolic chirp and the following silence with a known sequence of 30 FH-BFSK symbols. (The transmissions

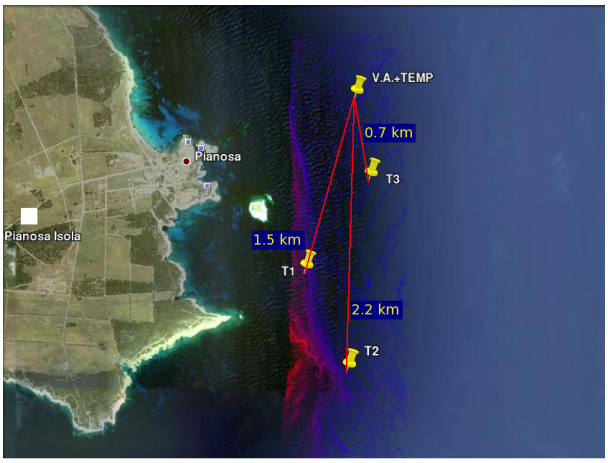

Figure 1. A scheme of the testbed deployment off the Pianosa Island (from [7]).

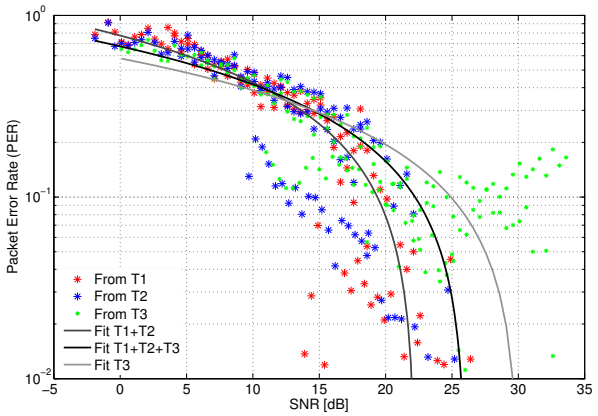

Figure 2. Log-scale scatterplot of PER as a function of SNR for varying transmitter and all receivers. Linear fits of the joint scatterplot of all transmitters as compared to the joint scatterplot of T1 and T2, as well as the scatterplot of T3, are also provided.

Table I
COEFFICIENTS OF PER FITTING LINES.

TX nodes	Slope (α)	Intercept (β)	MSE (same TX)	MSE (all TX)
T1+T2	-0.035	0.775	0.0101	0.0164
T1+T2+T3	-0.026	0.676	0.0136	0.0136
T3	-0.019	0.580	0.0095	0.0197

considered in this paper include no payload.) JANUS signals are partially protected from errors by means of physical-layer (PHY) Forward Error Correction (FEC), implemented through fixed interleaving and a rate-1/2 convolutional channel code of generating polynomials $(753_8, 561_8)$. In addition, the frequency hopping sequence is designed to escape multipath patterns featuring long delay spread.

The location of the experiments was chosen to be the island of Pianosa, Italy (42.585°N, 10.1°E). The testbed consisted of four hydrophones arranged at different depths in a vertical array (VA), and of three acoustic modems (all Teledyne-Low Frequency models [8]) placed on a tripod on the sea floor at a depth of 60, 70 and 80 m, at different distances from the VA (1500 m, 2200 m and 700 m, respectively). A scheme of the testbed is depicted in Figure 1 [7]. The three transmitters have been labeled T1 (1500 m from the VA, depth 60 m), T2 (2200 m from the VA, depth 70 m) and T3 (700 m from the VA, depth 80 m). The hydrophones of the VA (named H1, H2 and H4),[1] are placed at 20, 40 and 80 m, respectively. Temperature sampling in the water column close to the VA was provided by a thermistor chain.

The trials we are focusing on in this paper took place between the end of May and the end of August 2009, and include more that 12000 transmissions, in different channel conditions. In [7], this data set was used for a study of the power-delay profile and time spread characteristics of the links between the modems and the hydrophones. Unlike in [7], in the following we directly study the process of packet errors in order to derive synthetic models for transmission performance. To this end, we will focus on a representative set of results including one experiment performed on May 30 and a second experiment carried out on August 30, respectively indicated as experiments A and B.

B. Analysis of SNR and packet error rate

We start by analyzing PER as a function of SNR for the JANUS waveforms being considered. The correctness of the packet is inferred through a CRC check at the receiver after standard processing, i.e., detection of signal probe, reconstruction of the hopping pattern, non-coherent detection of BFSK symbols, de-interleaving and soft Viterbi decoding of the PHY-level convolutional code. Fig. 2 plots PER against SNR for all experiments listed in the previous subsection, for all transmitter-receiver links. The figure has been obtained by considering SNR bins of size 0.5 dB and by calculating the relative frequency of packet errors for all packets whose SNR falls in the same bin. Different markers and colors correspond to different transmitters. Fig. 2 also includes a linear regression fitting the relationship between PER and SNR expressed in dB, i.e.,

$$\text{PER} = \alpha \cdot \text{SNR} + \beta. \tag{1}$$

A negative-slope line adequately fits data in this case, in accordance to the approximate performance of incoherent BFSK detection in the high SNR regime and in the presence of frequency-flat fading (recall that the frequency hopping pattern is designed to mitigate the effects of multipath). Fig. 2 suggests that the closest link (i.e., from T3, in green) yields different performance with respect to the links from T1 and T2: this is due to the harsher multipath, whereby secondary paths yield significant power with respect to the main arrival. As a consequence, the line that fits only the outcomes from T3 (light grey) has lower slope than the other lines. Depending on the required degree of accuracy, one may decide to use the T1+T2+T3 fit, which considers data from all transmitters while providing an acceptably higher MSE with respect to the MSE of the linear fit of T3 points (see Table I).

As a first approximation, we may incorporate fitted PER curves into a simulator so as to reproduce the PER for matching modulation and receiver processing and in similar

[1] H3, placed at a depth of 60 m, experienced malfunctioning, therefore its recordings were not considered in our study.

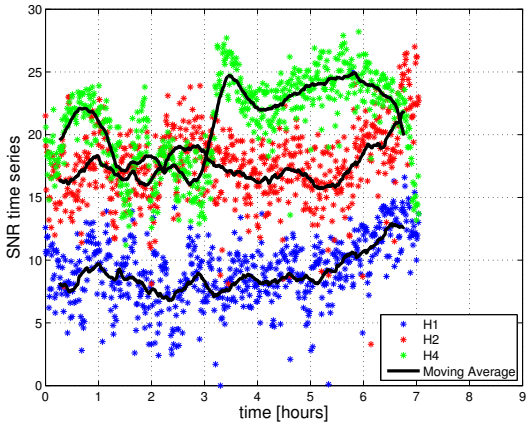

Figure 3. Time series of SNR for transmissions from T2 during experiment A. Moving averages over 50 samples are provided as a solid black line.

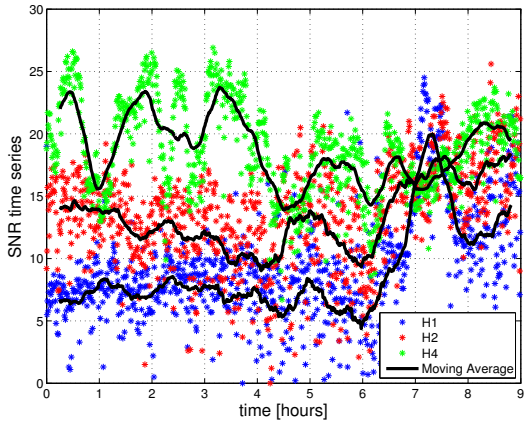

Figure 4. Time series of SNR for transmissions from T2 during experiment B. Moving averages over 50 samples are provided as a solid black line.

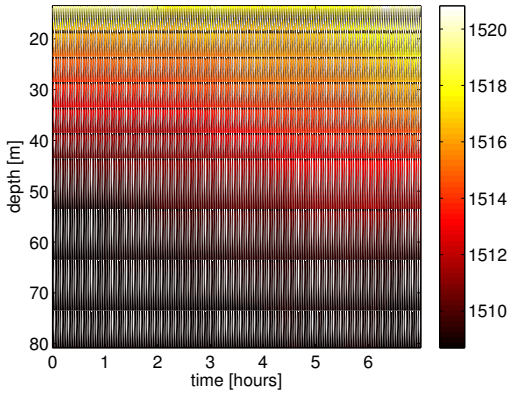

Figure 5. Sound speed profile [m/s] at different depths as a function of time during experiment A.

environments as the shallow summer waters of Pianosa. However, we would still need to factor in the correlation among SNR values, including those experienced between the same fixed transmitter and receiver: assuming uncorrelated SNR realizations may actually be too strong an assumption. This is exemplified in Figs. 3 and 4, which show the SNR time series for the signals transmitted by T2 during experiments A and B, respectively, as received by all hydrophones of the VA. For better clarity, a moving average over 50 samples of the trace is also shown as a solid black line. The figures show that some links are quite stable throughout the duration of the experiment, whereas others experience greater instability. For instance, the T2–H1 link in Fig. 3 is stable almost throughout the whole experiment, with the exception of a slight increase towards the end, as we will explain later. The same applies to the T2–H2 link as well. On the contrary, the T2–H1 link in Fig. 4 remains stable around an average SNR of 7 dB for roughly 6 hours, then experiences an abrupt improvement as its SNR increases to more than 20 dB, before falling back to roughly 13 dB. Similar observations apply to the T2–H2 link as well. Some oscillations of up to 10 dB in the value of SNR over the T2–H4 link can be observed in both figures; however it should be noted that the SNR remains very high, hence oscillations are not expected to have a significant impact on PER. We will elaborate on this point in the next section.

The most significant variations on the SNR in Figs. 3 and 4 cannot be ascribed to noise, because different hydrophones of the VA are differently affected. To give at least a partial explanation, we must therefore observe the time series of the sound speed at different depths (SSP) in the water column close to the VA.[2] Fig. 5 reports the sound speed samples taken every two minutes for the whole duration of experiment A. We observe a sound speed increase in the upper water layers from 6 to 7 hours after the beginning of the experiment; this changes the way acoustic waves are refracted, and in this case allows more power to be bent toward hydrophones closer to the surface (H1 and H2). For the same reason the SNR over the T2–H4 link decreases (H4 is the deepest hydrophone). Unfortunately, due to thermistor chain down time, we cannot display a similar plot for experiment B.

The variations of the average SNR over macroscopic time scales discussed above motivates us to analyze whether such variations can be profitably tracked through synthetic models such as Markov models (MMs) and hidden Markov models (HMMs), which incorporate memory of past events. The following section is devoted to the discussion of their applicability to the proposed scenario.

III. Markov models

To keep track of channel memory, we consider three different models, whose parameters are estimated from the measured data: a 2-state Markov channel, which keeps memory of one previous event (MM1); an extension of the same model bearing a memory of 2 previous events and resulting in a 4-state channel (we will refer to this model as MM2), and a 2-state hidden Markov model (HMM). The accuracy of these models is then compared to an independent and identically

[2]We recall that the testbed deployment included a thermistor chain, which is used to indirectly measure sound speed at different depths by virtue of the Mackenzie formula [9] and by assuming that water salinity does not vary significantly throughout the summer season.

distributed (iid) error model and to real channel traces.[3] To evaluate the accuracy of the models, we consider the predicted average error probability ε, the probability mass function (pmf) of the length of an error burst (i.e., the probability $p_b(k)$ that the number b of consecutive errors (i.e., an error burst) is equal to k) and the m-step error correlation (i.e., the probability $\xi_{n,m} = \mathbb{P}[\text{packet } n+m \text{ erroneous}|\text{packet } n \text{ erroneous}]$). We choose these metrics because i) the average error probability ε is the primary check for the correctness of an estimated model; ii) an accurate approximation of the pmf of error bursts is important to assess the impact of the model on network protocols, in addition to being tightly related to the chosen model (e.g., a 2-state Markov model exhibits a geometric burst length pmf [11]); finally iii) second-order statistics such as the m-step error correlation $\xi_{n,m}$ have a significant impact on network protocols and may lead to design guidelines (e.g., protocols should not insist on transmitting over a channel whose errors are still highly correlated for high m).

A. 2-state Markov model (MM1)

This model is characterized by two states, labeled 0 and 1, which represent a correct and erroneous packet reception, respectively. The model is specified by the transition matrix

$$\mathbf{P}_2 = \begin{pmatrix} p_{00} & p_{01} \\ p_{10} & p_{11} \end{pmatrix}, \tag{2}$$

which regulates the transitions between correct and wrong receptions, and where the subscript 2 refers to the number of states. Let us call $\boldsymbol{\pi} = [\pi_0 \ \pi_1]$ the vector containing the steady-state distribution of the Markov chain, i.e., the solution to the system of equations $\pi_j = \sum_i \pi_i p_{ij}$ under the constraint that $\sum_i \pi_i = 1$. In this case, the error probability is $\varepsilon_2 = \pi_1 = p_{01}/(p_{01}+p_{10})$; moreover, we have $p_b(k) = p_{11}^{k-1} p_{10}$, and $\xi_{n,m} = p_{1,1}^{(m)}$, where $p_{1,1}^{(m)}$ is the element in position $(1,1)$ of the m-step transition matrix, $\mathbf{P}_2^m$.

B. 4-state Markov model with memory of two past events (MM2)

This model expands the 2-state model by explicitly incorporating further memory of past events within states. Four states are defined, i.e., (00), (01), (10) and (11), where 0 and 1 represents again a correct and a wrong packet reception; the transition probabilities between these states are thus arranged into a 4×4 matrix $\mathbf{P}_4$, with elements of the kind $p_{(k-1\ k),(k\ k+1)}$, where the event with index k is in common between the pair before and after the transition. In this case, the average probability of error is $\varepsilon = \pi_{01} + \pi_{11}$; the pmf of the burst length is found by considering the evolution of the Markov process from the only state leading to errors after a successful packet reception, i.e., state (10):

$$p_b(k) = \begin{cases} p_{01,10} & k = 1 \\ p_{01,11} p_{11,11}^{k-2} p_{11,10} & k \geq 2 \end{cases} \tag{3}$$

[3]The MM1 model was also considered in a comparative study [10] focused on N-states Markov channel models, where however the number of states tracks changes in the SNR level instead of providing explicit memory of past error events as in this paper; in addition, we note that the study in [10] considers an iso-velocity medium and trains models using simulated channel traces instead of field measurements.

Similarly, $\xi_{n,m}$ is found as

$$\xi_{n,m} = \frac{\pi_{01}\left(p_{01,01}^{(m)} + p_{01,11}^{(m)}\right) + \pi_{11}\left(p_{11,01}^{(m)} + p_{11,11}^{(m)}\right)}{\pi_{01} + \pi_{11}}. \tag{4}$$

C. 2-state hidden Markov model (HMM)

HMMs assume that a non-observable state structure lies beneath observed values for a certain random process [12]. In this case, we observe erroneous or correct packet reception, and make the assumption that the probability of such events actually depends on the (hidden) state of the channel. As in the hidden Gilbert-Elliot model [13], [14], the state may represent a different level of goodness of the channel, corresponding to a different probability of receiving a packet correctly.

HMMs can be described in terms of a transition probability matrix $\mathbf{P}_H$ (whose structure is the same as $\mathbf{P}_2$ in this case); furthermore, by defining $\phi_i(j)$ as the probability that event j is observed in state i, we can define the following diagonal observation probability matrices

$$\mathbf{C} = \begin{pmatrix} \phi_0(0) & 0 \\ 0 & \phi_1(0) \end{pmatrix} \quad \mathbf{E} = \begin{pmatrix} \phi_0(1) & 0 \\ 0 & \phi_1(1) \end{pmatrix}, \tag{5}$$

which respectively model correct (matrix $\mathbf{C}$) and erroneous (matrix $\mathbf{E}$) packet reception in either state [11], [12]. Since the state of the chain is hidden, all statistics must be averaged through the stationary distribution of the underlying Markov process.

Therefore, the average probability of error is $\varepsilon = \boldsymbol{\pi}\mathbf{E}\,\mathbf{e}$, where $\mathbf{e} = [1\ 1]^T$, and we recall that $\boldsymbol{\pi}$ is the steady-state probability distribution vector of the hidden Markov chain. In addition, we remark that the matrix products $\mathbf{P}_H\mathbf{E}$ and $\mathbf{P}_H\mathbf{C}$ yield the joint probability of making a transition and observing an erroneous or correct packet, respectively, *after* the transition has been completed. The burst length probability distribution can be found in accordance to the previous definitions:

$$p_b(k) = \frac{\boldsymbol{\pi}\mathbf{C}(\mathbf{P}_H\mathbf{E})^k\mathbf{P}_H\mathbf{C}\,\mathbf{e}}{\boldsymbol{\pi}\mathbf{C}\mathbf{P}_H\mathbf{E}\,\mathbf{e}} \tag{6}$$

The conditional probability $\xi_{n,m}$ is found by considering m-step spaced error events, by averaging over the probability of being initially in state 0 or 1, and by conditioning on the event that an error was in fact observed on the initial state, i.e.,

$$\xi_{n,m} \quad = \quad \frac{\boldsymbol{\pi}\mathbf{E}\mathbf{P}_H^m\mathbf{E}\,\mathbf{e}}{\boldsymbol{\pi}\mathbf{E}\,\mathbf{e}}, \tag{7}$$

where we note that both terms of the fraction are scalar.

D. Comparison among Markov models and channel traces

We begin by comparing the average probability of successful packet reception, $1-\varepsilon$, as predicted by the models and as measured from data traces. This test is a basic check that the models are correct; in addition, it is worth noting that a simple slotted Stop-and-Wait Automatic Repeat reQuest (ARQ) protocol would exhibit a throughput of $1-\varepsilon$ packets per round-trip time. The results of the evaluation are reported in Table II and show good accordance with measurements.

Consider now the m-step error correlation $\xi_{n,m}$ defined in Section III. Figs. 6 and 7 show this metric for the links between T2 and all hydrophones during experiments A and

B, respectively. The figures compare $\xi_{n,m}$ as predicted by all models against the probability of having an erroneous packet using an iid model and against measured traces. The pictures suggest that non-hidden models perfectly reproduce short-term correlation (i.e., where their inherent memory of past errors allows a correct representation of the channel behavior); however, they converge very quickly to their stationary behavior, as indicated by the fact that predicted error correlation quickly reaches the iid floor; on the contrary, the HMM achieves a much better reproduction of long-term error correlation, at the price of only a slight error in the short-term correlation.

By comparing the results of Figs. 6 and 7 to those in Figs. 3 and 4, we can note that channel traces are not always representative of a hidden model. For example, the T1–H1 and T2–H2 links in Fig. 3 are quite stable even on a long time scale, and can be successfully modeled by non-hidden approaches as well. Conversely, such links as T2–H4 in Fig. 3 as well as all links in Fig. 4 exhibit much larger oscillations, which an HMM is expected to capture more effectively. Figs. 6(c) and 7(a)–(c) confirm this intuition by showing that HMMs adhere better to measured error correlation values on the long term. Indeed, while in some cases HMMs also converge to the iid floor faster than measured data (e.g., Figs. 7(a) and 7(b)), they do so more slowly than non-hidden models do.

Table II
COMPARISON OF AVERAGE CORRECT PACKET RECEPTION PROBABILITIES

Receiver	Data	MM1	MM2	HMM
Experiment A				
H1	0.578	0.580	0.579	0.580
H2	0.569	0.568	0.567	0.568
H4	0.924	0.923	0.922	0.910
Experiment B				
H1	0.370	0.369	0.369	0.369
H2	0.690	0.692	0.691	0.695
H4	0.924	0.923	0.922	0.910

The goodness of HMMs is also suggested by the observation of the pmf of the length of an error burst, $p_b(k)$. We focus again on transmitter T2 and on experiments A and B, whose results are reported in Figs. 8 and 9. These figures compare $p_b(k)$ as predicted by the models against the pdf estimated from real data (represented by red star-shaped markers). The figures show that in general the best approximation of data is yielded by MM2, followed by HMM and MM1, with occasionally similar performance on some of the links. To further support this assertion, we have reported in the legend of each picture the Kullback-Leibler divergence (KLD) of predicted pmfs from the pmf estimated from data traces. In almost all cases the divergence is smaller for the MM2 and HMM models than for the MM1 and iid models, with the exception of Fig. 8(b), where the KLD of the HMM slightly exceeds that of non-hidden models. Along with the satisfactory approximation of long-term error correlation, this suggests that HMM models are good candidates for a synthetic model of acoustic channels. We remark that we have focused only on transmissions from T2 in experiments A and B, but these results are representative of all other experiments and links,

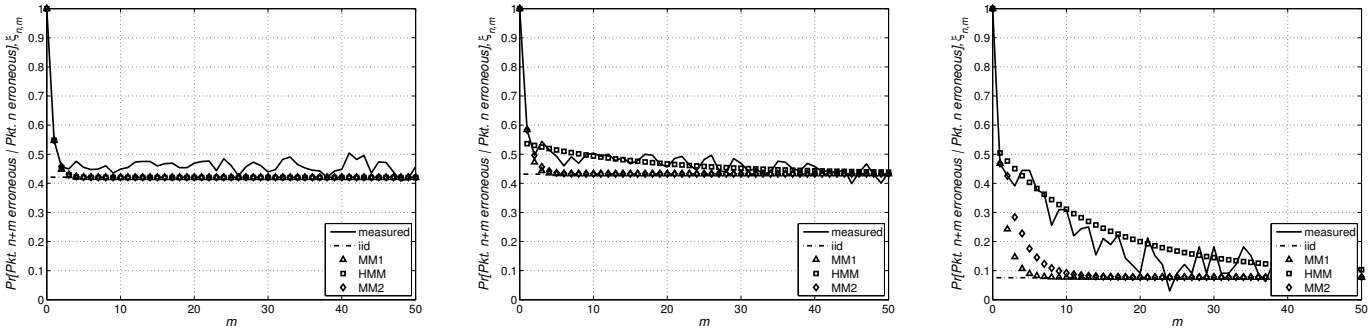

(a) Link T2–H1. (b) Link T2–H2. (c) Link T2–H4.

Figure 6. m-step error correlation. Transmitter T2, experiment A.

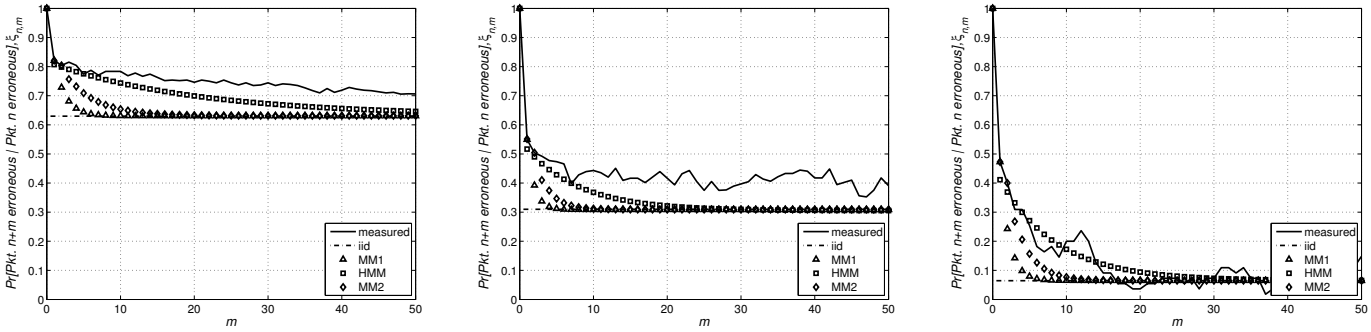

(a) Link T2–H1. (b) Link T2–H2. (c) Link T2–H4.

Figure 7. m-step error correlation. Transmitter T2, experiment B.

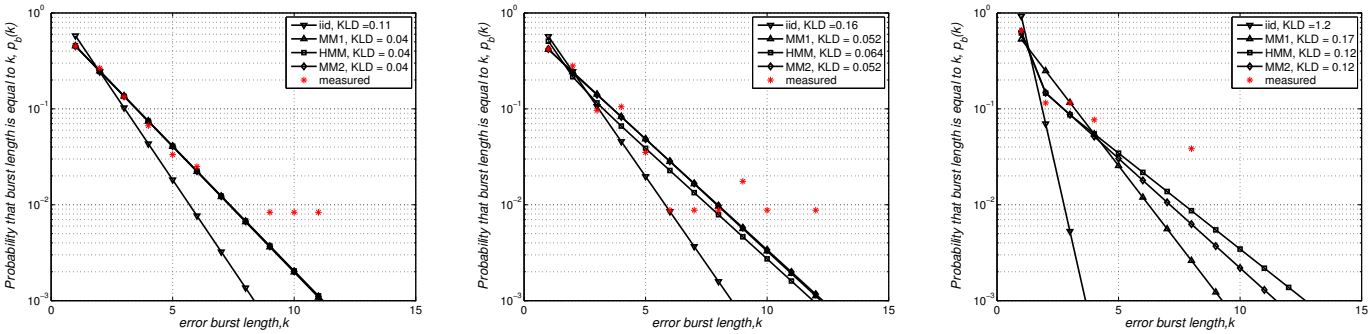

(a) Link T2–H1. (b) Link T2–H2. (c) Link T2–H4.

Figure 8. Probability of observing k consecutive errors. Transmitter T2, experiment A.

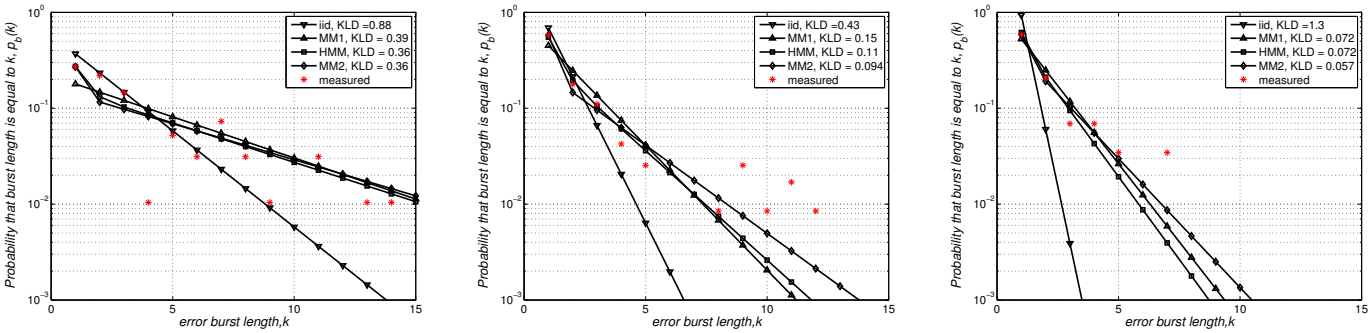

(a) Link T2–H1. (b) Link T2–H2. (c) Link T2–H4.

Figure 9. Probability of observing k consecutive errors. Transmitter T2, experiment B.

which would allow to draw the same conclusions.

IV. Conclusions

In this paper we have presented an evaluation and comparison of channel models for a shallow-water acoustic channel in the waters near the Pianosa island, Italy. The transmission format was JANUS, a FH-BFSK-based format with PHY-level FEC implemented through a convolutional code. We considered Markov models with memory of both one and two past events, and a hidden Markov model (HMM), and compared them to data traces and a simpler iid error model. Our comparison shows that the HMM is better at tracking long term channel behavior, especially if substantial shifts between low quality and high quality channel states are observed; in addition, an HMM yields a much better representation of long-term error correlation, while providing a very good approximation of the distribution of the length of error bursts.

As a final note, we remark that other datasets may certainly be considered to train the same type of Markov models considered in this study. However, we focused on the SubNet'09 dataset because it contains long experimental runs: this makes it possible to assess the model accuracy in channels experiencing limited non-stationarity due to changing environmental conditions. Future work on this topic includes implementing the models in a more complex network simulator and validating the results using different datasets.

Acknowledgment

This work has been supported in part by the NATO Undersea Research Center under contracts no. 40800700 (ref. NURC-010-08) and 40900654, and by the Italian Institute of Technology within the Project SEED framework.

References

[1] J. Partan, J. Kurose, and B. Levine, "A survey of practical issues in underwater networks," in *Proc. of ACM WUWNet*, Los Angeles, CA, Sep. 2006.

[2] "Aqua-Sim: An NS2 based Underwater Sensor Network Simulator." [Online]. Available: http://ubinet.engr.uconn.edu/mediawiki/index.php/Aqua-Sim

[3] J.-M. J. Montana, "AUVNetSim: A Simulator for Underwater Acoustic Networks." [Online]. Available: http://users.ece.gatech.edu/jmjm3/publications/auvnetsim.pdf

[4] F. Guerra, P. Casari, and M. Zorzi, "World Ocean Simulation System (WOSS): a simulation tool for underwater networks with realistic propagation modeling," in *Proc. of WUWNet 2009*, Berkeley, CA, Nov. 2009.

[5] M. Zorzi and R. R. Rao, "On channel modeling for delay analysis of packet communications over wireless links," in *Proc. of 36th Allerton Conf.*, Monticello, IL, Sep. 1998.

[6] K. McCoy, "JANUS: from primitive signal to orthodox networks," in *Proc. of IACM UAM*, Nafplion, Greece, Jun. 2009.

[7] B. Tomasi *et al.*, "Experimental study of the space-time properties of acoustic channels for underwater communications," in *Proc. IEEE/OES Oceans*, Sydney, Australia, May 2010.

[8] "Teledyne benthos undersea systems and equipment," www.benthos.com.

[9] K. V. Mackenzie, "Nine-term equation for the sound speed in the oceans," *J. Acoust. Soc. Am.*, vol. 70, no. 3, pp. 807–812, 1981.

[10] F. Pignieri, F. De Rango, F. Veltri, S. Marano, "Markovian approach to model underwater acoustic channel: techniques comparison," in *Proc. of IEEE MILCOM*, San Diego, Nov. 2008.

[11] W. Turin and R. van Nobelen, "Hidden Markov Modeling of Flat Fading Channels," *IEEE J. Sel. Areas Commun.*, vol. 16, no. 9, pp. 1809–1817, Dec. 1998.

[12] L. R. Rabiner, "A tutorial on hidden Markov models and selected applications in speech recognition," in *Proc. of the IEEE*, 1989, pp. 257–286.

[13] E. N. Gilbert, "Capacity of a Burst-noise Channel," *Bell Systems Tech. Journal*, vol. 39, pp. 1253–1266, Sep. 1960.

[14] E. O. Elliot, "Estimates of Error Rates for Codes on Burst-error channels," *Bell Systems Tech. Journal*, vol. 42, pp. 1977–1997, Sep. 1963.